A "eye-in-body" integrated surgery robot system for stereotactic surgery

A “eye-in-body” integrated surgery robot system for stereotactic surgery

Cite this article as: Liang Li, Julia Wu, Hui Ding and Guangzhi Wang, A “eye-in-body” integrated surgery robot system for stereotactic surgery, International Journal of Computer Assisted Radiology and Surgery https://doi.org/10.1007/s11548-019-02032-x

A “eye-in-body” integrated surgery robot system for stereotactic surgery

Liang Li[a] ·Julia Wu[a,b] ·Hui Ding[a] ·Guangzhi Wang[a*]

a Department of Biomedical Engineering, School of Medicine, Tsinghua University, Beijing 100084, China

b Department of Electrical Engineering and Computer Science, Massachusetts Institute of Technology, Cambridge, Massachusetts, USA

Liang Li

Postal address: Room C249, School of Medicine, Tsinghua University, Beijing, P.R. China, 100084

Telephone: 86-181-5621-2205

Fax: 86-10-6279-4377

Email: lil17@mails.tsinghua.edu.cn

Julia Wu

Postal address: Room C249, School of Medicine, Tsinghua University, Beijing, P.R. China, 100084

Telephone: +1 650-483-6342

Fax: 86-10-6279-4377

Email: juliawu@mit.edu

Hui Ding

Postal address: Room C249, School of Medicine, Tsinghua University, Beijing, P.R. China, 100084

Telephone: 86-10-6278-3631

Fax: 86-10-6279-4377

Email: dinghui@tsinghua.edu.cn

*Guangzhi Wang (Corresponding author)

Postal address: Room C249, School of Medicine, Tsinghua University, Beijing, P.R. China, 100084

Telephone: 86-10-6278-3631, 86-139-0109-3926

Fax: 86-10-6279-4377

Email: wgz-dea@tsinghua.edu.cn

A "eye-in-body" integrated surgery robot system for stereotactic surgery

Liang Li[a] ·Julia Wu[a,b] ·Hui Ding[a] ·Guangzhi Wang[a*]

a Department of Biomedical Engineering, School of Medicine, Tsinghua University, Beijing 100084, China

b Department of Electrical Engineering and Computer Science, Massachusetts Institute of Technology, Cambridge, Massachusetts, USA

*Guangzhi Wang (Corresponding author)

Email: wgz-dea@tsinghua.edu.cn

Abstract

Purpose: Current stereotactic surgical robots system relies on cumbersome operations such as calibration, tracking and registration to establish the accurate intraoperative coordinate transformation chain, which makes the system not easy to use. To overcome this problem, a novel stereotactic surgical robot system has been proposed and validated.

Methods: First, a hand-eye integrated scheme is proposed to avoid the intraoperative calibration between robot arm and motion tracking system. Second, a special reference-tool-based patient registration and tracking method is developed to avoid intraoperative registration. Third, a model-free visual servo method is used to reduce the accuracy requirement of hand-eye relationship and robot kinematic model. Finally, a prototype of the system is constructed and performance tests and a pedicle screw

drilling experiment are performed.

Results: The results show that the proposed system has acceptable accuracy. The target positioning error in the plane is -0.68 ± 0.52 mm and 0.06 ± 0.41 mm. The orientation error was 0.43 ± 0.25°. The pedicle screw drilling experiment shows that the system can complete accurate stereotactic surgery.

Conclusions: The stereotactic surgical robot system described in this paper can perform stereotactic surgery without the intraoperative hand-eye calibration and nor manual registration and can achieve an acceptable position and orientation accuracy while tolerating the errors in the hand-eye coordinate transformation error and the robot kinematics model error.

Keywords Stereotactic surgery; Surgical robotics; Model-free control; Patient tracking; Patient registration; Image guided intervention;

1. Introduction

Robot-assisted stereotactic surgery is increasingly being valued clinically for its accuracy and stability [1,2]. In stereotactic surgery, the patient's anatomy and surgical plan can vary, the patient may shift and move, and the robotic arm may also be shifted. Therefore, an external motion tracking system is usually used to establish the intraoperative coordinate transformation chain between a plurality of objects such as the image, surgical path, robot arm, and surgical tool. To guarantee the accuracy of coordinate transformation chain, cumbersome intraoperative operations such as

calibration, tracking and registration are required, which makes the system not easy to use and may introduce unnecessary sources of error. Therefore, the motivation of this work is to reduce the amount and accuracy requirement of above operations during the robot-assisted stereotactic surgery. There are three main areas where the above ideas can be implemented: the motion tracking system and robot arm calibration (hand-eye calibration), patient tracking, and robotic control.

Hand-eye calibration is essential for stereotactic surgical robots. In current existing research[3,4], the motion tracking system is usually separated from the robot and tracks while remaining fixed relative to the robot base coordinate system (eye-to-hand). This requires accurate transformation of the robot arm base coordinate system to the motion tracking coordinate system. However, because the motion tracking system can only track its markers and not the robotic arm base coordinate system itself, the transformation cannot be directly acquired. Thus, the surgeon needs to calibrate the positional relationship between the tracking marker fixed on the robot arm and the robot arm base coordinate system before the operation. This lengthens the operation time and introduces human calibration errors. There are also some studies which integrate the tracking system with the robotic arm base (eye-in-body) [5,6]. However, these systems still require markers to find the relationship between their tracking system and their robot arm. Thus, such systems still need the above hand-eye calibration step.

Patient tracking is required to compensate for the movement of the patient during the operation. Establishing the coordinate transformation relationship between the

tracking marks and the surgical path is essential for ensuring effective motion compensation. Some methods require the pre-calibration of the robotic arm and the patient, resulting in a longer coordinate transfer chain. They must first register the coordinate relationship between the surgical path and the robot arm by using the CT image, and then use the motion tracking system to find the transformation between the robot arm and the patient tracking mark [4,7]. The coordinate transformation chain can be shortened by using the CT image to directly establish the coordinate relationship between the patient tracking marker and the surgical path. Because the position of the tracking mark is difficult to obtain directly using the CT image, additional image fiducials such as screws or beads are usually used as a bridge to connect the tracking system space and the CT image space. In some studies, the position relationship between the image fiducial and the tracking mark needs to be registered manually in every surgery [8,9]. Although these manual operations can ensure tracking accuracy, they can be time consuming [10]. A more convenient method is still needed to establish the coordinate relationship between the patient tracking marker and the surgical path.

There are currently two main methods for the control of stereotactic robots. The control system calculates the surgical path in the base coordinate system of the robot arm based on all coordinate transfer chains, and reaches the target pose using the kinematics of the robot arm [4,5]. The other is visual servo control [11,12]. This requires accurate mathematical models, which in turn requires strict calibration of the hand-eye relationship and robot kinematics model. Model-free visual servo methods

do not rely on a precise hand-eye calibration nor an accurate arm kinematics model [13,14]. However, the convergence of this method is highly sensitive to the initial values of the control algorithm[15]. Whether this method is suitable for stereotactic robots still needs further exploration.

The goal of this paper is trying to reduce the amount and accuracy requirement of some operations when establishing the intraoperative coordinate transformation chain, thereby achieving an easy-to-use stereotactic surgical robot system. In this paper, we design a hand-eye integrated scheme for stereotactic surgical robot system, present an automatic method to find the patient-tracker registration chain, study the model-free visual servo control method, verify the system accuracy that can be achieved, and confirm the feasibility of the scheme.

2. Method

2.1 System overview

An "eye-in-body" hand-eye integrated robotic system (Fig. 1a) is designed. The motion tracking system is fixed to the waist (first joint link) of the robot arm and can be pitched by a stepper motor, as shown in Fig. 1b and Fig. 1c. A patient reference tool (Fig. 1d) consisting of four steel registration beads and a tracking marker is designed such that the tracking marker and image fiducial have a determinable spatial positional relationship. In addition, a guiding tool (Fig. 1e) with four tracking markers and four guiding holes is also designed.

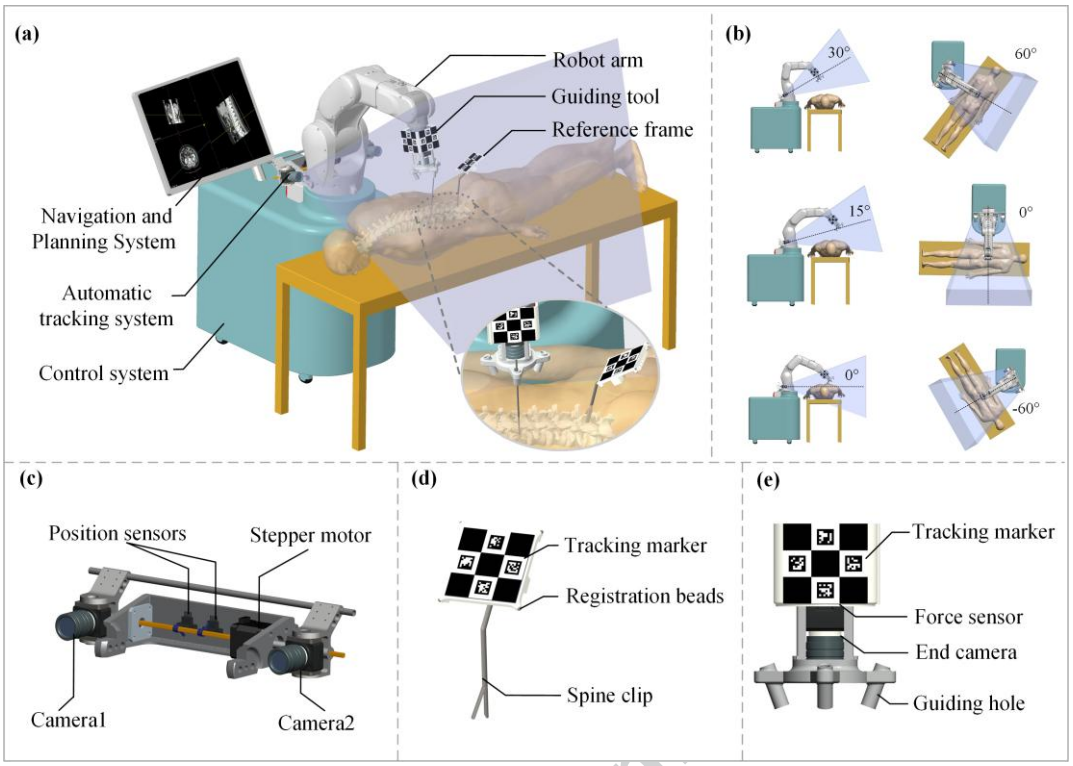

Fig. 1 Overview of the proposed system. **a** System component, taking spinal surgery as an example. **b** The motion tracking system can rotate horizontally and pitch vertically. **c** Motion tracking system components. **d** Patient reference tool. **e** Guiding tool components

The coordinate transfer chain of the system is shown in Fig. 2. In the trackable surgical path definition stage, the reference tool was first fixed to the patient's anatomy and the patient was scanned using CT. The relationship (1) between the surgical path and image fiducials in image space is calculated from the CT image. The relationship (2) between image fiducials and tracking marker in patient space is fixed and can be obtained ahead of time. In the stereotactic operation stage, the pose (3) of tracking marker on the reference tool is obtained by intraoperative tracking. Thus, the surgical path in patient space can be registered to the motion tracking system

automatically. The pose (4) of guiding tool can also be tracked at the same time. The deviation of orientation and position between the surgical path and guiding tool in motion tracking system space is the input to the system controller. Using this deviation, a model-free control method controls the robotic arm to move the guiding tool along the surgical path. The hand-eye relationship (5) and the robot arm kinematic model (6) are used to provide initial parameters to model-free control method. The hand-eye relationship can be calculated based on our hand-eye integrated scheme. The robot arm kinematic model can be established from factory parameters. Thus, during the surgery, the interoperative coordinate transfer chain can be automatic established only need tracking step (3) and (4), which significantly reduced the amount of intraoperative operations. Furthermore, benefit to the model-free control method, the accuracy requirement of hand-eye relationship and robot arm kinematic model can also be reduced.

The following sections will describe the above issues in hand-eye integration, patient path registration and tracking and robot system control.

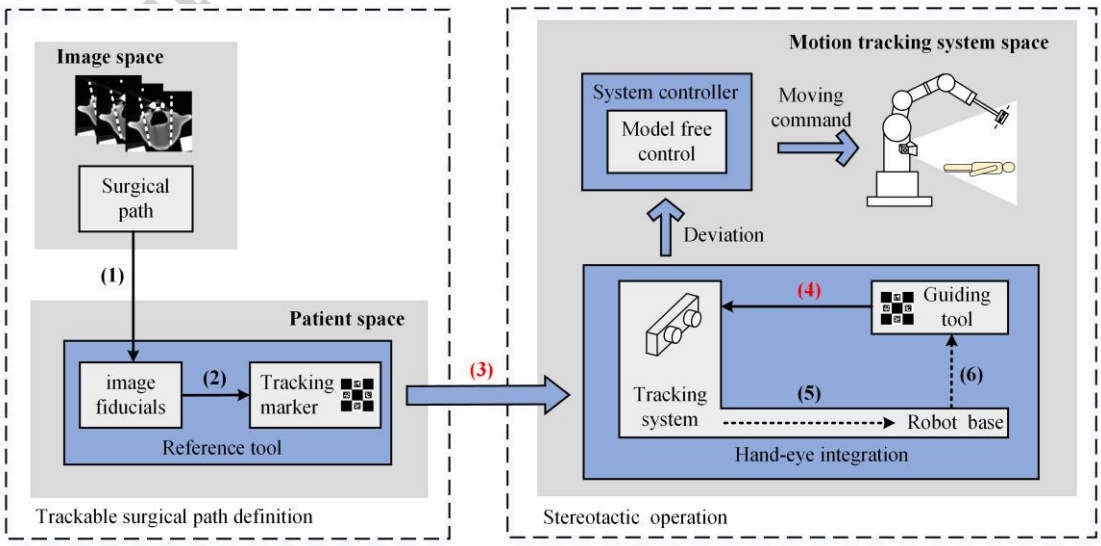

Fig. 2 The coordinate transfer chain of the proposed system. (1) the transformation from the planned surgical path to image fiducials, (2) the transformation from image fiducials to tracking marker, (3) the transformation from tracking marker to motion tracking system, (4) the transformation from the guiding tool to the motion tracking system, (5) the transformation from robot arm base to motion tracking system, (6) the transformation from the robot arm base to the guiding tool.

2.2 Hand-eye integration

2.2.1 Motion Tracking System

The motion tracking system is used to monitor the motion of both the robot and the patient. Two monocular cameras are used to construct a stereo vision motion tracking system. A chessboard planar fiducial pattern (ChArUco) is used as the tracking marker [16]. Reconstruction of the three-dimensional coordinates of the marked corner points by a stereo vision algorithm can achieve accurate tracking of spatial position and pose. The stereo vision tracking method used follows reference [17]. The process of stereo vision calibration used follows reference [18].

To mount and setup, the two cameras are first fixed on the shaft of a stepper motor. The stepper motor and position sensors are used to pitch the camera's angle of view, as shown in Fig. 1c. Then the camera-motor system is mounted on the first joint link of the robot arm to rotate horizontally together with the first joint of the robot arm, as shown in Fig. 3a. This mounting setup ensures that the guiding tool is always within

the tracking system's field of view. The view angle of tracking system can be actively controlled, which gives the tracking system more flexibility.

2.2.2 Hand-eye relationship calculation

Because the motion tracking system is connected to the robot arm base by two rigid links and two rotating joints and there are two rotational degrees of freedom (as seen in Fig. 3a.), the hand-eye relationship transformation matrix can be automatically calculated based on forward kinematics, as shown in (1).

$$^{base}T_{cam} = {}^{base}T_{link1}\,{}^{link1}T_{link2}\,{}^{link2}T_{cam} \tag{1}$$

Where, $^{base}T_{cam}$ is the coordinate transformation matrix between the tracking system and the robot arm base coordinate system. $^{base}T_{link1}$ is the coordinate transformation matrix between link 1 and the robot arm base coordinate system, represented by formula (2). $^{link1}T_{link2}$ is the coordinate transformation matrix between link 2 and link 1, represented by formula (3). $^{link2}T_{cam}$ is a coordinate transformation matrix between the tracking system and link 2.

$$^{base}T_{link1} = R_{z_{link1}}(\theta_1) \tag{2}$$

$$^{link1}T_{link2} = R_{z_{link1}}(\theta_{cam})T_{z_{link1}}(d)T_{x_{link2}}(a)R_{x_{link2}}(\alpha) \tag{3}$$

Formula (2) and (3) are established based on the Devanit-Hartenberg (DH) method [19]. In formula (2), $^{base}T_{link1}$ contains only one rotation transformation of the robot's first joint angle θ_1. In formula (3), $^{link1}T_{link2}$ is a function of camera pitch angle θ_{cam} and contains three DH parameters including two translation parameters d, a and a rotation parameter α. The θ_1 and θ_{cam} can be read directly from the system controller. The parameters d, a, α and $^{link2}T_{cam}$ can be found using standard DH

parameters calibration methods[19]. This calibration only needs to be done once when the system is manufactured. Because hand-eye relationship only used to provide initial parameters to model-free control method, high calibration accuracy is not required.

2.3 Patient registration and tracking

The transformation matrix between the surgical path and tracking system cameras ${}^{cam}T_{path}$ is necessary for patient tracking. As shown in Fig. 3b, the matrix can be calculated using formula (4).

$$ {}^{cam}T_{path} = {}^{cam}T_{marker}\,{}^{marker}T_{bead}\,{}^{bead}T_{path} \tag{4} $$

Where ${}^{cam}T_{marker}$ is the transformation from the tracking markers to the motion tracking system, ${}^{marker}T_{bead}$ is the transformation from the registration beads to the tracking marke, ${}^{bead}T_{path}$ is the transformation from the surgical path to the registration beads

The conversion matrix ${}^{bead}T_{path}$ is established from CT images, where the reference tool and patient were simultaneously scanned by the intraoperative CT imaging system. During the patient tracking phase, the robot uses the motion tracking system to measure the coordinate transformation matrix ${}^{cam}T_{marker}$.

To obtain the transformation matrix ${}^{marker}T_{bead}$, four steel registration beads are fixed at the tip of the reference tool (Fig. 1e). Due to this structure, the position of each registration beads under the tracking marker coordinate system can be obtained by the pivot method[20], thereby the transformation matrix for all registration beads

can be obtained. Because ${}^{marker}T_{bead}$ is a fixed matrix, this step only needs to be done once when the tool is made. Thus, the transformation matrix between the surgical path and tracking system cameras can be established without interoperative manual measuring.

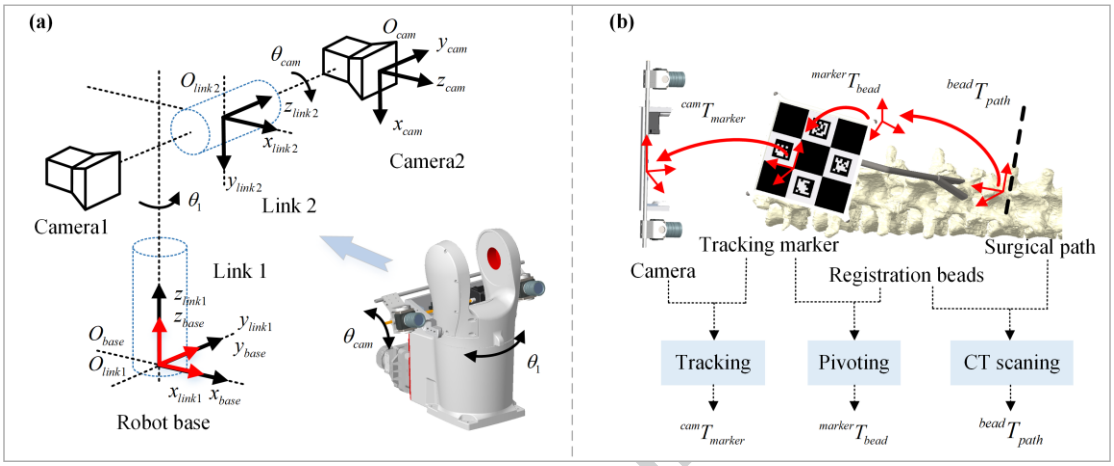

Fig. 3 Hand-eye integration and patient registration and tracking. **a** Coordinate relationship in hand-eye relationship calculation. **b** Coordinate relationship from patient to tracking system in patient registration and tracking.

2.4 Robot system control

2.4.1 Control strategy

In this paper, we use a model-free control method to execute the planned surgical path during surgery, which reduce the accuracy requirement of robot kinematics model and a hand-eye relationship. The control process is shown in Fig. 4a. It consists of three stages. In the first stage, the coordinate transfer chain (Fig. 4b) is used to coarse control the robot arm to reach a pose near the target orientation and position. This stage provides the initial orientation and position for the next two stages. In the second stage, the model-free control method is used to fine-tune the orientation. In the

final stage, model-free control is used again to control the robot arm to reach the target position tracking a linear path.

2.4.2 model-free control

The basic idea of the model-free control method used is to observe the deviation between the current position and orientation and the target position and orientation directly in the tracking system space. Then this deviation is used to estimate the control Jacobian matrix online. The deviation matrix of position and orientation can be calculated according to Fig. 4b. In order to further enhance the convergence and stability of the control algorithm, the control of position and orientation are implemented separately using the model-free method in robot task space. The framework of model-free control is shown in Fig. 5.

During the orientation control stage, the orientation deviation is expressed in the form of a rotation vector (from the rotation part of matrix ${}^{tool}T_{patient}$), and the actuation change is the orientation of the robot flange. The orientation deviation is minimized iteratively using the static Quasi-Newton method. The Jacobian matrix used in the static Quasi-Newton method is estimated using static Broyden's method [15]. This method can estimate the Jacobian matrix according to the response of the deviation to the control variable instead of using a precis model base analytical Jacobian matrix.

During the position control stage, the robot arm is controlled to follow a linear trajectory to the target position. As shown in Fig. 4a, the points between the initial position and the target position are linearly interpolated, and each interpolation point is set as a dynamic target. The robot tracks each dynamic target, gradually reaching

the final target position in a linear trajectory. The dynamic Quasi-Newton method is used for dynamic tracking. The Jacobian matrix in the dynamic Quasi-Newton method is estimated by dynamic Broyden's method [15].

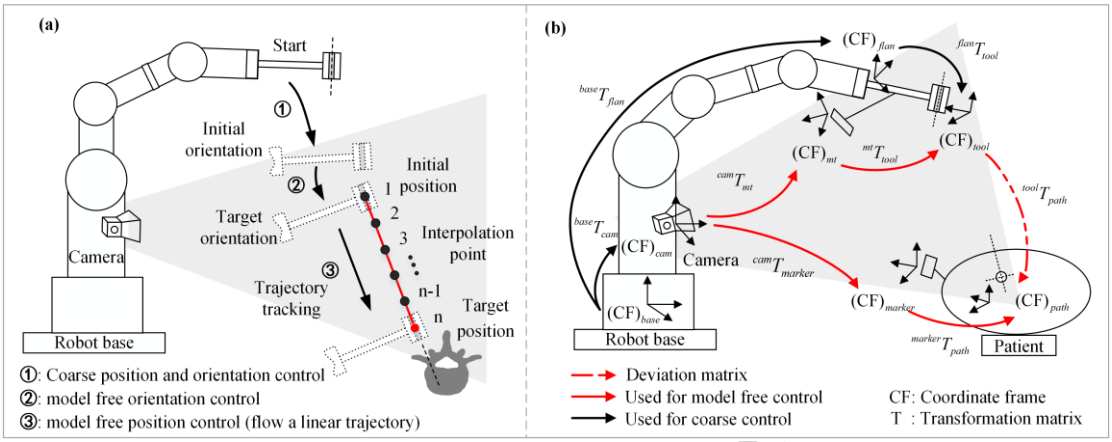

Fig. 4 Control strategy and coordinate transfer relationship of the system. **a** The control process, split into stages 1, 2 and 3. **b** System coordinate transfer diagram; In stage 1, the tracking system cameras to robot base transfer matrix ${}^{base}T_{cam}$ is obtained as described in section 2.2, the surgical path to tracking system cameras transfer matrix ${}^{cam}T_{path}$ is obtained as described in the section 2.3, the guidance tool transformation matrix ${}^{tool}T_{flan}$ can be obtained through tool calibration; the transformation matrix of the robotic arm ${}^{base}T_{flan}$ is the actuation variable. Note that due to the limited accuracy of each link, there is still a large control error by using this coordinate transfer chain; In stages 2 and 3, the orientation deviation and position deviation is derived from deviation matrix ${}^{tool}T_{path}$. The ${}^{tool}T_{path}$ is calculated using the difference between the pose matrix of the guiding tool ${}^{cam}T_{tool}$ and the pose matrix of the target surgical path ${}^{cam}T_{path}$. ${}^{cam}T_{tool}={}^{cam}T_{mt}\,{}^{mt}T_{tool}$ is obtained through guiding tool tracking and calibration. ${}^{cam}T_{path}$ is obtained in the coarse control stage.

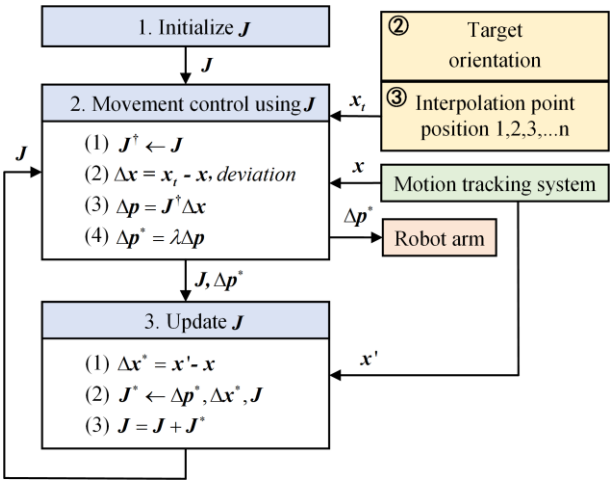

Fig. 5 Framework of model-free control based on estimate Jacobian matrix. During model-free control, the actuation change $\Delta \boldsymbol{p}$ is calculated from deviation $\Delta \boldsymbol{x}$ and pseudo-inverse of Jacobian $\boldsymbol{J}^{\dagger}$ in robot task space, and scaled by damping ratio λ to get real change $\Delta \boldsymbol{p}^{*}$ (Quasi-Newton method). The initial Jacobian $\boldsymbol{J}$ is derived from coarse coordinate transfer chain. For update of $\boldsymbol{J}$, matrix $\boldsymbol{J}^{*}$ is derived from real task space change $\Delta \boldsymbol{x}^{*}$ (Broyden's method). In the orientation control stage, the actuation change $\Delta \boldsymbol{p}$, target $\boldsymbol{x}_t$, tracking variable $\boldsymbol{x}$, deviation $\Delta \boldsymbol{x}$ are rotation vector, the target $\boldsymbol{x}_t$ is the target orientation[13]. In the position control stage, the actuation change $\Delta \boldsymbol{p}$, target $\boldsymbol{x}_t$, tracking variable $\boldsymbol{x}$, deviation $\Delta \boldsymbol{x}$ are position in cartesian coordinates, the target $\boldsymbol{x}_t$ is a dynamic trajectory point[21].

2.5 Prototype system

A prototype system (Fig. 6a) is built in this paper using a robot arm (VS060A3, Denso Co. Ltd., Japan), a motion tracking system with two cameras (BFLY-U3-28S4C, FLIR Integrated Imaging Solutions, Inc, Canada), a stepper motor (42BYGH47-1684B-ZK6, Liko Inc, China), and two position sensors (EE-SX672WR,

Omron Co. Ltd, Japan). Each camera has a resolution of 1928 × 1448 and lens focal length of 8mm. Connecting parts are manufactured by 3D printing. The robot controller software is built using Qt, OpenCV, Eigen and other software packages. The relationship of the tracking system field of view and robot working range is shown in Fig. 6b.

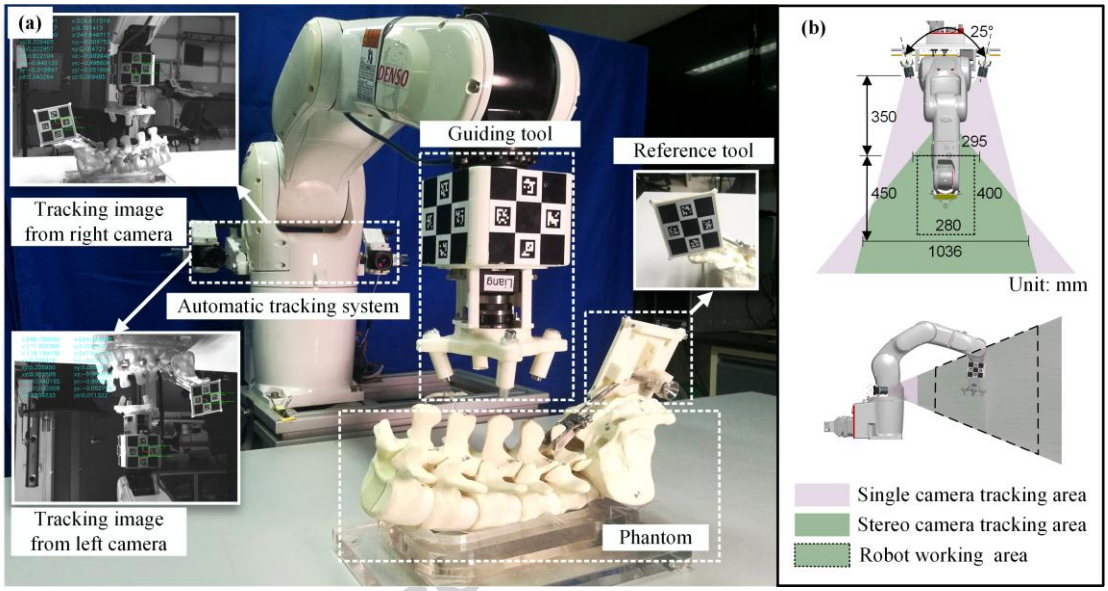

Fig. 6 Prototype system overview. **a** Prototype robot system. **b** Tracking system field of view and robot working range

3. Experiments and results

First, the performance of the system prototype was tested (sections 3.1, 3.2, 3.3). Second, the drilling step of pedicle screw placement surgery was used as an example to verify system functionality (section 3.4).

3.1 Hand-eye integration experiments and results

To test the performance of the hand-eye integration method, we first verified the

tracking accuracy of motion tracking system, then verified the accuracy of hand-eye relationship calculation.

3.1.1 Motion tracking system accuracy verification

We tested the accuracy of the stereo vision motion tracking system at different distances from the marker. The spatial position of the square corner of the ChArUco marker center was reconstructed at 6 different distances, and the marker's edge length and angle were calculated as shown in Fig. 7. The distances were chosen within the range of 350mm-600mm. Each position was measured 10 times. The result is shown in Table 1, the gold standard of length was 22 mm, and the angle is 90°. The distance accuracy is better than 0.16 mm. The angle accuracy is better than 0.23°.

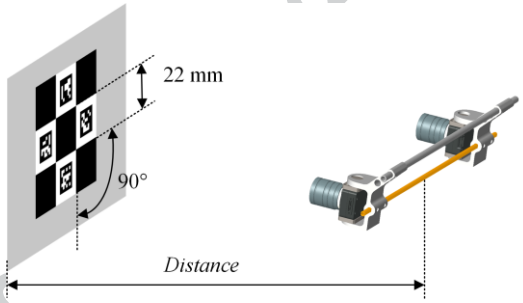

Fig. 7 Reconstruction of ChArUco marker by the motion tracking system

Table 1 Reconstruction accuracy of the motion tracking system

Distance (mm)	350	400	450	500	550	600
Length (mm)	21.90	21.94	21.97	22.00	22.01	22.01
SD (mm)	0.06	0.03	0.01	0.01	0.01	0.02
Angle (°)	90.00	90.00	90.02	90.03	89.99	89.98
SD (°)	0.23	0.17	0.15	0.10	0.06	0.04

3.1.2 Hand-eye relationship calculation accuracy verification

To test the accuracy of our hand-eye relationship calculation method, the robot arm was controlled to carry the tracking marker around the workspace following a set trajectory. The position of the marker is measured by both the motion tracking system and the robot controller. The difference in measurements in the *XYZ* direction and L2 distance (Euclidean distance) was found. These differences theoretically should all be zero because the hand-eye relationship calculation makes the tracking system and robot arm share the same coordinate system. The selected measurement area was a square array in the robot arm workspace. 48 positions were measured, as shown in Fig.8. The coordinate transformation matrix from the markers to the robot arm flange was previously calibrated using the method by Tsai [20].

Table 2 shows the test results. The conversion error between the tracking system and the mechanical base arm coordinate system is within ± 1.47 mm in the selected measurement area. This result shows our hand-eye relationship calculation method can provide a rough hand-eye relationship for model-free robot arm control.

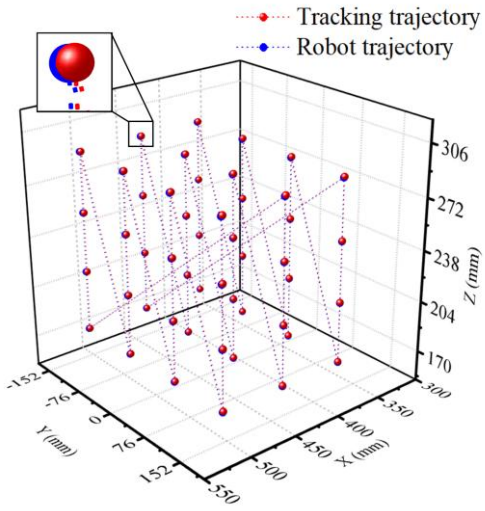

Fig. 8 Hand-eye calculation accuracy verification experiments, comparison of position difference between the spatial trajectories of the two measurement modes.

Table 2 Error of the hand-eye relationship calculation

Direction	*X*	*Y*	*Z*	L2
Mean error (mm)	0.53	-0.03	-0.51	1.00
SD (mm)	0.33	0.40	0.64	0.47

3.2 Patient registration and tracking experiment and result

To test the performance of the patient registration and tracking method, we first verified the pivoting accuracy of the patient reference tool, then verified the registration process and accuracy on a spine phantom.

3.2.1 Pivoting accuracy of the patient reference tool

First, the position of the four registration beads in the marking coordinate system was determined by the pivot method[20]. Then, the optical tracking system (Optotrak Certus, 3D Accuracy 0.1 mm, Northern Digital Inc, Canada) was used to measure the

spatial position of the registration beads in the optical tracking system coordinate frame (optical system probe calibration error 0.14 mm), as a gold standard (Fig. 9). After registering the spatial locations measured by the two methods, the registered fiducial registration error (FRE) was used to evaluate the pivoting accuracy of patient reference tool. Each registration bead was repeatedly measured 10 times in the marker coordinate system and the average repeatability was 0.16 mm. Each registration bead was repeatedly measured 5 times by the optical tracking system, and the average repeatability was 0.11 mm. The final registration FRE was 0.68 ± 0.21 mm.

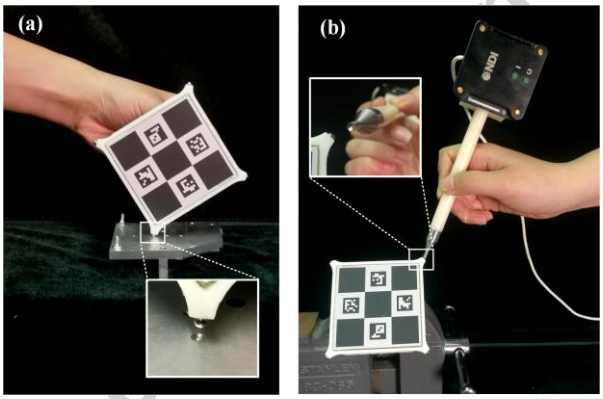

Fig. 9 Reference tool calibration accuracy evaluation. **a** Getting the position of the registration beads using the pivot method. **b** Getting the position of the registration beads using optical tracking system

3.2.2 Phantom registration and accuracy verification

A spine phantom was prepared. The phantom was composed of a reference tool, a sawbone lumbar spine phantom, and target steel beads (Fig. 10a). The reference tool was fixed to the first lumbar vertebra by a spinal clip. The lumbar spine was composed of L1~L5 vertebrae and a sacrum(S). There are 20 total target steel beads

with a diameter of 2.5 mm fixed on the L1~L5 vertebral and sacrum; three steel beads were fixed per vertebrae and five were fixed on the sacrum.

To perform registration, the phantom was first scanned by CT. The 3-dimensional CT image of the phantom is shown in Fig. 10(b), 10(d). The imaging resolution is 0.442 mm × 0.442 mm × 1 mm. The volume data of each registration beads in the image was automatically segmented by the threshold method. The position of this beads was set as the centroid of the segmented volume. The position of the surgical path relative to the registration beads was calculated in the image space. Since the position of the registration beads in the tracking marker coordinate system is already known, the surgical path can be automatically registered to the tracking marker.

The registration accuracy was evaluated using the target steel bead mounted on the vertebrae and sacrum. The true spatial position of the registration beads and target steel bead was measured by the Certus optical tracking system. The position of beads in the CT image was also extracted by the centroid method mentioned above. The position of registration beads in the CT coordinate system was registered to the position in the optical tracking system. The FRE and target registration error (TRE) of the registration beads and the target steel bead was calculated in the same coordinate system. Each steel bead was measured 5 times by the optical tracking system as shown in Fig. 10c. The resulting FRE was 0.30 ± 0.10 mm, the TRE was 0.59 ± 0.20 mm. The TRE distribution of each vertebra was shown in Table 3. The overall registration error was under 1 mm.

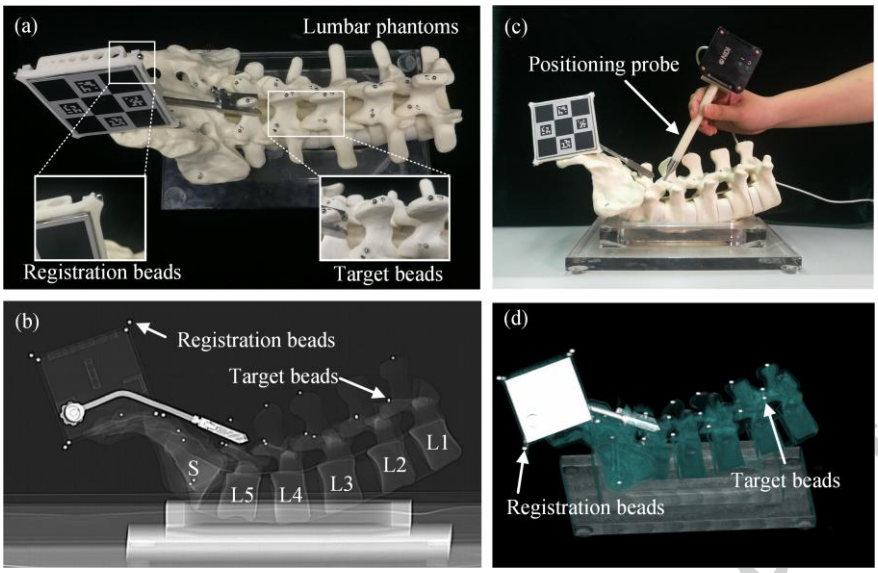

Fig. 10 Registration accuracy verification experiment. **a** Lumbar spine phantom. **b** The CT image. **c** Measuring the true spatial position of the steel beads using the optical tracking system. **d** 3D model of the phantom

Table 3 TRE in different vertebra

Vertebrae	Mean TRE (mm)	Max TRE (mm)
L1	0.86±0.06	0.92
L2	0.73±0.12	0.84
L3	0.44±0.19	0.64
L4	0.39±0.13	0.46
L5	0.47±0.09	0.58
S	0.64±0.15	0.86

3.3 Robot system control experiments and results

The position and orientation accuracy of the entire system as a whole was tested.

Convergence experiments were also implemented to study the robustness of our system to different initial conditions.

3.3.1 Position and orientation accuracy evaluation

First, a linear probe tool was used to set the target position and direction for robot system. At the same time, the pose of the linear probe tool was measured by Certus optical tracking system, as shown in Fig. 11a. Then the robot system was controlled to the target pose. After the robot reaches the target pose, the probe tool was inserted into the guide hole and the pose of the probe tool was measured again by Certus optical tracking system, as shown in Fig. 11b. The target error and orientation error were calculated by comparing these two measurements. 20 different targets in a measurement grid were tested. The target position was set in the center of the grid and the target orientation was set randomly for each trial. The termination threshold of orientation and position was 0.6°and 0.5 mm.

The position error in the *X* direction of optical tracking system was -0.68 ± 0.52 mm. The position error in the *Y* direction was 0.06 ± 0.41 mm. The orientation error was 0.43 ± 0.25°. Fig. 11c shows the target error distribution. The total time consumption in each test was 89±11s.

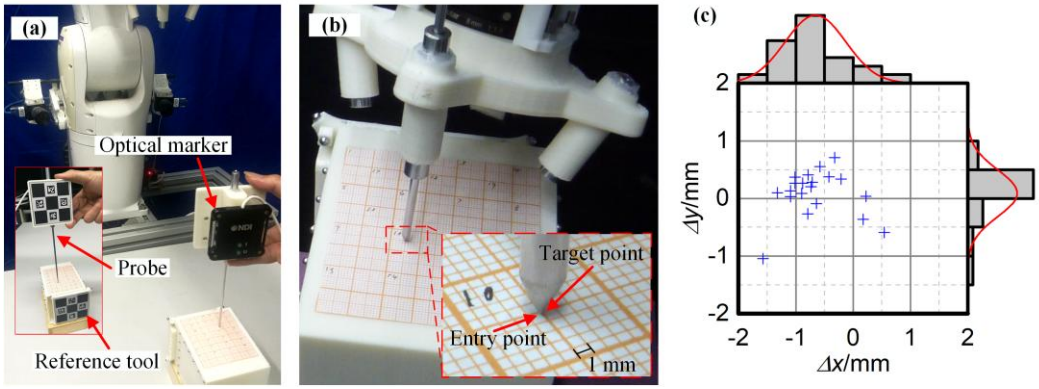

Fig. 11 Position and orientation accuracy verification experiment. **a** The probe tool was used to set the target position and direction, the optical marker of Certus optical tracking system was used as a gold stand to record the target value. **b** Arrival position and direction accuracy measurement. **c** Position error distribution in *X* direction and *Y* direction.

3.1.2 Convergence of robot control system

Different levels robot kinematic model error was artificially added by applying different amplitudes of rotation and translation noise to the transformation matrix between the guide hole and the robot flange. The resulting noisy kinematic model was used to control the robot arm to an initial orientation and position, then model-free control of orientation and position were implemented separately. The number of iterations and convergence time was recorded to analyze the convergence. In the orientation control experiments, the rotation angle noise was set at a total of ten different levels ranging from 0° to 18°. At each noise level, 10 random orientation targets were selected. The iteration termination threshold was set to 0.6°. In the position control test, the translation noise also had ten levels ranging from 0 mm to 45 mm. At each noise level, 10 random position targets were selected. The robot first used the kinematic model reach to an initial position 100mm away from the target, and then moved to the final target position by tracking the linear interpolation points. The number of interpolation points was 10, and the stopping threshold was set to 0.5mm.

Both the orientation control and the position control converge despite various different noise levels as shown in Fig. 12a and Fig. 12b. The final orientation deviation is 0.46 ± 0.11 °, and the final position deviation is 0.38 ± 0.10 mm. The iteration steps and the convergence time under different noise amplitudes is shown in Fig. 12c and Fig. 12d. It can be seen that, in orientation control, the number of iteration steps and the convergence time increase with the model rotation noise. However, in position control, due to the existence of the linear interpolation, there is no significant difference between the iteration step and the convergence time, but the standard deviation becomes significantly larger, which indicates that as the translation noise increases the stability of the convergence speed deteriorates. The above results show that the model-free control method used in our system has a certain tolerance to initial condition error, and that the more accurate the model used with coarse positioning control, the better the convergence of the model-free control.

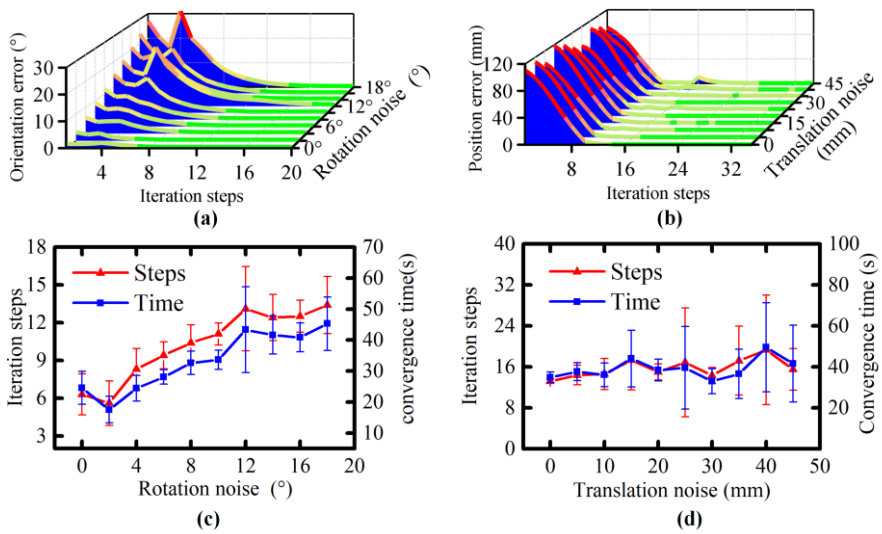

Fig. 12 Convergence of system control. **a** Orientation deviation between the robot arm and the target orientation across iterations under different rotational noise, green lines

mean the deviation is under the stopping threshold. **b** Position deviation between the robot arm and the target position across iterations under different translational noise. **c** Steps and time to convergence under different rotation noise in model-free orientation control. **d** Steps and time to convergence under different translation noise in model-free position control

3.4 Drilling experiments and result

To verify the proposed system's functionality, we used the system to perform pedicle screw drilling on the above spine phantom. The surgical path was planned in the CT image in using 3D Slicer software. The registration between the surgical path and the patient reference tool was done in the above section. The phantom was first placed in the robotic arm workspace visible to the motion tracking system. Then, the robot moved to the pose corresponding to the desired surgical path. Finally, the operator completes the pedicle drilling operation using the guide hole, as shown in Fig. 13a. After the operation, the phantom was scanned by CT again at the same resolution. The centroid of the target steel bead was used to fusion this image to the preoperative CT image containing the planned path. The fusion images were then used to evaluate the drilling accuracy. The actual drilling entry point and axis were manually determined in 3D Slicer, and the lateral error, axial error, and deviation of angle were calculated as shown in Fig. 13b.

10 planned surgical paths were implemented, 5 each on the left and right sides of the L1-L5 vertebrae. The iteration stop threshold was 0.5 mm, and the registration

FRE was 1.08±0.61 mm. The results are shown in Table 4 (The image fusion FRE was 0.34±0.19 mm).

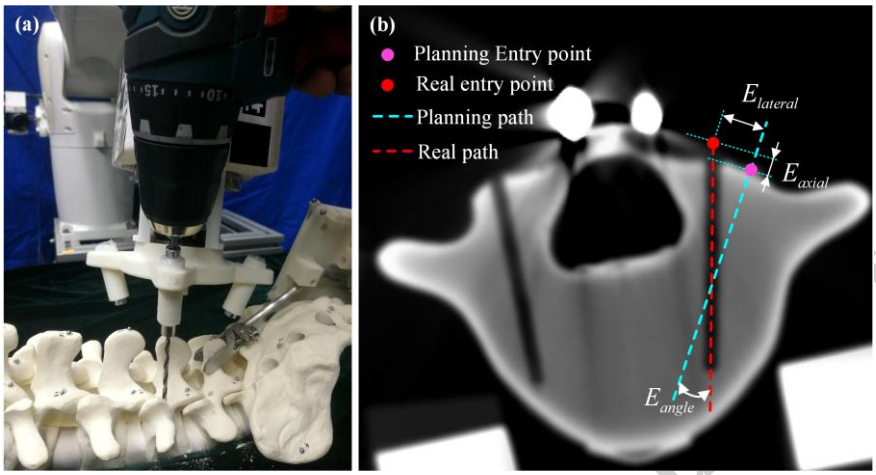

Fig. 13 Drilling experiment. **a** Pedicle screw drilling. **b** The CT image of vertebral image after drilling and the definition of the lateral error $E_{lateral}$, axial error E_{axial}, and deviation of angle E_{angle}

Table 4 Accuracy of drilling experiment

Experiment number	Vertebra and side	$E_{lateral}$ (mm)	E_{axial} (mm)	E_{angle} (°)
1	L1-L	0.89	-0.63	0.37
2	L1-R	0.73	-1.34	0.38
3	L2-L	1.26	0.46	0.72
4	L2-R	2.80	-2.84	1.30
5	L3-L	2.20	1.40	1.39
6	L3-R	2.05	0.40	0.11

7	L4-L	2.24	2.66	0.74
8	L4-R	1.75	0.41	1.80
9	L5-L	1.20	0.29	1.75
10	L5-R	1.44	-0.10	1.95
Mean error	-	1.66	0.07	1.05
SD	-	0.67	1.48	0.67

4. Discussion

In this paper, we proposed a stereotactic surgery robotic system and verify its performance and feasibility. The system allows for hand-eye integration, reference tool based patient registration, and model-free control. The hand-eye integrated scheme can calculate the hand-eye relationship directly, avoiding interoperative hand-eye calibration. The reference tool based patient registration method can register the surgical path to reference tool automatically, avoiding intraoperative manual registration. The mode-free control method can achieve an acceptable accuracy while tolerating errors in the hand-eye coordinate transformation and errors in the robot kinematics model.

Automatically finding the transformation matrix between the image fiducial and the tracking marker is key to direct patient tracking. Some studies use manufacturer specifications to calculate this matrix, but this relies on the quality of manufacturing [22,23]. In this paper, the custom reference tool structure allows for the coordinate relationship between the registration beads and the tracking marker to be determined

using only the pivot method[20]. Because, the pivot operation is simple, easy to use and have a promising accuracy, our method is effective to find the transformation matrix between the image fiducial and the tracking marker at the early stages of concept validation.

Finding good initialization parameters, which is important for stability and convergence, is usually a challenge for model-free control [21,13]. In our system, all coordinate transfer parameters can be coarsely calibrated at the manufacturing stage. These parameters provide a good initial position for model-free control, and also provides a good initial value for the Jacobian matrix in the Broyden's algorithm. The experiments in Fig. 12 demonstrate that this control scheme can achieve stable and accurate control using these coarse parameters, which shows the suitability of model-free control for stereotactic robots.

Experiments in convergence of robot control show Broyden's algorithm has increased sensitivity to large kinematic model error. Although coarse control using a rough coordinate transfer chain can provide acceptable initial conditions and ensure control robustness experimentally, more theoretical methods, such as the Lyapunov method [14,24], are still needed to further analyze the stability boundary of this method.

The results of Sections 3.3 show our system can provide a position and orientation accuracy under 1mm and 1°, but the error in the drilling experiment has large deviations. This is because of the “uneven terrain” of vertebral bone. Even with the help of the guiding hole, the drill bit will still slip on the vertebrae when manually

drilling. This implies that in addition to positioning and orientation guidance, stereotactic robots should have better autonomous operation capabilities, avoiding additional errors caused by manual operations. The automatic drilling operation in cochlear implantation robot [11] is a successful example. For our system, similar functions can be further explored in the future.

5. Conclusion

In this paper we proposed a stereotactic surgery surgical robot system using a hand-eye integrated scheme, a specially designed patient reference tool and a model-free robot control method. Using our proposed system and method, the amount of intraoperative hand-eye calibration and manual registration steps can be significantly reduced, while not drastically decreasing accuracy compared to both conventional hand-eye and robot kinematics coordinate transfer chains.

Acknowledgement The authors acknowledge the support of the Ministry of Science and Technology of China (Grant 2017YFA0205904, 2016YFC0105800).

Compliance with ethical standards

Conflict of interest The authors declare that they have no conflict of interest.

Ethical approval This article does not contain any studies with human participants or animals performed by any of the authors.

Informed consent This article does not contain patient data.

References

1. Ghasem A, Sharma A, Greif DN, Alam M, Al Maaieh M (2018) The Arrival of Robotics in Spine Surgery A Review of the Literature. Spine 43 (23):1670-1677. doi:10.1097/brs.0000000000002695

2. Fomenko A, Serletis D (2017) Robotic Stereotaxy in Cranial Neurosurgery: A Qualitative Systematic Review. Neurosurgery. doi:10.1093/neuros/nyx576

3. Tian W (2016) Robot-Assisted Posterior C1-2 Transarticular Screw Fixation for Atlantoaxial Instability A Case Report. Spine 41 (19B):B2-B5. doi:10.1097/brs.0000000000001674

4. Lefranc M, Peltier J (2016) Evaluation of the ROSA Spine robot for minimally invasive surgical procedures. Expert Rev Med Devices 13 (10):899-906. doi:10.1080/17434440.2016.1236680

5. Khan A, Meyers JE, Siasios I, Pollina J (2018) Next-Generation Robotic Spine Surgery: First Report on Feasibility, Safety, and Learning Curve. Operative neurosurgery (Hagerstown, Md). doi:10.1093/ons/opy280

6. Bell B, Stieger C, Gerber N, Arnold A, Nauer C, Hamacher V, Kompis M, Nolte L, Caversaccio M, Weber S (2012) A self-developed and constructed robot for minimally invasive cochlear implantation. Acta Oto-Laryngol 132 (4):355-360. doi:10.3109/00016489.2011.642813

7. Song J, Ding H, Han W, Wang JQ, Wang GZ (2016) A motion compensation method for bi-plane robot-assisted internal fixation surgery of a femur neck fracture. Proc Inst Mech Eng Part H-J Eng Med 230 (10):942-948.

doi:10.1177/0954411916663582

8. Danilchenko A, Balachandran R, Toennies JL, Baron S, Munske B, Fitzpatrick JM, Withrow TJ, Webster RJ, Labadie RF (2011) Robotic Mastoidectomy. Otol Neurotol 32 (1):11-16. doi:10.1097/MAO.0b013e3181fcee9e
9. Tian W, Han XG, Liu B, Liu YJ, Hu Y, Han X, Xu YF, Fan MX, Jin HY (2014) A Robot-Assisted Surgical System Using a Force-Image Control Method for Pedicle Screw Insertion. PLoS One 9 (1):9. doi:10.1371/journal.pone.0086346
10. Gerber N, Gavaghan KA, Bell BJ, Williamson TM, Weisstanner C, Caversaccio MD, Weber S (2013) High-Accuracy Patient-to-Image Registration for the Facilitation of Image-Guided Robotic Microsurgery on the Head. Ieee Transactions on Biomedical Engineering 60 (4):960-968. doi:10.1109/tbme.2013.2241063
11. Weber S, Gavaghan K, Wimmer W, Williamson T, Gerber N, Anso J, Bell B, Feldmann A, Rathgeb C, Matulic M, Stebinger M, Schneider D, Mantokoudis G, Scheidegger O, Wagner F, Kompis M, Caversaccio M (2017) Instrument flight to the inner ear. Sci Robot 2 (4):12. doi:10.1126/scirobotics.aal4916
12. Tauscher S, Fuchs A, Baier F, Kahrs LA, Ortmaier T (2017) High-accuracy drilling with an image guided light weight robot: autonomous versus intuitive feed control. Int J Comput Assist Radiol Surg 12 (10):1763-1773. doi:10.1007/s11548-017-1638-x
13. Jin YS, Wang YF, Chen XT, Wang ZC, Liu XH, Jiang H, Chen XP (2017) Model-Less Feedback Control for Soft Manipulators. In: Bicchi A, Okamura A

(eds) 2017 Ieee/Rsj International Conference on Intelligent Robots and Systems. IEEE International Conference on Intelligent Robots and Systems. Ieee, New York, pp 2916-2922

14. Wang HS, Jiang MK, Chen WD, Liu YH (2012) Visual servoing of robots with uncalibrated robot and camera parameters. Mechatronics 22 (6):661-668. doi:10.1016/j.mechatronics.2011.05.007
15. Piepmeier JA, Mcmurray GV, Lipkin H A dynamic quasi-Newton method for uncalibrated visual servoing. In: IEEE International Conference on Robotics and Automation, 1999. Proceedings, 1999. pp 1595-1600 vol.1592
16. Danying H, DeTone D, Chauhan V, Spivak I, Malisiewicz T (2018) Deep ChArUco: Dark ChArUco Marker Pose Estimation arXiv. arXiv (USA):11 pp.-11 pp.
17. Lin Q, Cai K, Yang R, Chen H, Wang Z, Zhou J (2016) Development and Validation of a Near-Infrared Optical System for Tracking Surgical Instruments. Journal of Medical Systems 40 (4):1-14
18. Liu X, Liu ZY, Duan GF, Cheng J, Jiang XT, Tan JR (2018) Precise and robust binocular camera calibration based on multiple constraints. Appl Optics 57 (18):5130-5140. doi:10.1364/ao.57.005130
19. Deacon G, Harwood A, Holdback J, Maiwand D, Pearce M, Reid I, Street M, Taylor J (2010) The Pathfinder image-guided surgical robot. Proc Inst Mech Eng Part H-J Eng Med 224 (H5):691-713. doi:10.1243/09544119jeim617
20. Fuhrmann AL, Splechtna R, Prikryl J (2001) Comprehensive calibration and

registration procedures for Augmented Reality. In: Frohich B, Deisinger J, Bullinger HJ (eds) Immersive Projection Technology and Virtual Environments 2001. Eurographics. Springer-Verlag Wien, Vienna, pp 219-227

21. Yip MC, Camarillo DB (2014) Model-Less Feedback Control of Continuum Manipulators in Constrained Environments. IEEE Trans Robot 30 (4):880-889. doi:10.1109/tro.2014.2309194
22. Wei J, Wang TM, Liu D (2011) A vision guided hybrid robotic prototype system for stereotactic surgery. Int J Med Robot Comput Assist Surg 7 (4):475-481. doi:10.1002/rcs.431
23. Lin QY, Yang RQ, Cai K, Si X, Chen XW, Wu XM (2016) Real-time automatic registration in optical surgical navigation. Infrared Phys Technol 76:375-385. doi:10.1016/j.infrared.2016.03.011
24. Li T, Zhao H, Chang Y (2018) Visual servoing tracking control of uncalibrated manipulators with a moving feature point. Int J Syst Sci 49 (11):2410-2426. doi:10.1080/00207721.2018.1504138